



Amine-modified Ni-DOBDC MOF for CO₂ capture: CO₂ adsorption capacity and reusability

Irsan Fahriansyah^{1,2}, Irena Khatrin^{1,2}, Iman Abdullah^{1,2}, Yuni Krisyuningsih Krisnandi^{1,2,*}

¹ Department of Chemistry, Faculty of Mathematic and Natural Sciences, Universitas Indonesia, Depok, West Java 16424, Indonesia;

² Solid Inorganic Framework Laboratory, Department of Chemistry, Faculty of Mathematic and Natural Sciences, Universitas Indonesia, Depok, West Java 16424, Indonesia.

*Correspondence: yuni.krisnandi@sci.ui.ac.id

ABSTRACT

Background: Anthropogenic carbon dioxide (CO₂) emissions have risen significantly due to the extensive use of fossil fuels, necessitating the development of effective CO₂ capture and conversion techniques. Adsorption using Metal-Organic Frameworks (MOFs) has shown great potential due to their high CO₂ adsorption capacity, particularly Ni-based MOFs. Enhancing their adsorption efficiency remains a key research focus to improve sustainability in CO₂ capture applications. **Methods:** Ni-based MOF (Ni-DOBDC) was synthesized using the solvothermal method, employing DMF as the solvent and 2,5-dihydroxyterephthalic acid (DOBDC) as the organic ligand. To enhance CO₂ adsorption capacity, Ni-DOBDC was further modified with ethylenediamine (EDA) via post-synthetic modification. Structural characterization was performed using XRD, confirming similarity to the Ni-DOBDC reference (CCDC 288477), and FTIR, which showed enhanced absorbance peaks. SEM-EDX analysis revealed a flower-like morphology with an average particle size of 0.75 μm. CO₂ adsorption tests were conducted on Ni-DOBDC and EDA/Ni-DOBDC (10%) using the titration method under controlled conditions. **Findings:** The CO₂ adsorption capacity of Ni-DOBDC and EDA/Ni-DOBDC was tested at 70°C with a CO₂ concentration of 50% in N₂. EDA modification significantly improved CO₂ adsorption capacity, with EDA/Ni-DOBDC achieving 9.95 mmol g⁻¹ compared to pristine Ni-DOBDC's 6.44 mmol g⁻¹. However, Ni-DOBDC exhibited better regeneration ability in a three-cycle reusability test, likely due to EDA leaching during regeneration. **Conclusion:** EDA-modified Ni-DOBDC demonstrates enhanced CO₂ adsorption capacity, making it a promising material for CO₂ capture applications. However, its reduced regeneration stability suggests the need for further optimization to improve long-term performance. Future studies should explore strategies to minimize EDA leaching while maintaining high adsorption efficiency. **Novelty/Originality of this article:** This study provides new insights into improving Ni-based MOF performance for CO₂ capture through post-synthetic modification with EDA. The findings highlight a trade-off between increased adsorption capacity and material stability, emphasizing the need for further refinement in MOF functionalization strategies.

KEYWORDS: Ni-DOBDC MOF; ethylenediamine; CO₂ adsorption; biogas model.

1. Introduction

The advancement of technology has led to an increase in energy demand, resulting in the rapid consumption of fossil fuels, which remain one of the primary energy sources worldwide (Stolar et al., 2021). The combustion of fossil fuels currently accounts for more than 85% of the global energy demand, and by 2040, that percentage is projected to increase by 30% (Ghanbari et al., 2020; Ullah et al., 2020). The overconsumption of fossil fuels is followed by the large emissions of greenhouse contributing CO₂ gas into the atmosphere. A sharp increase in atmospheric CO₂ concentration has been observed, rising from 278 ppm to 415 ppm in 2019, marking a 6.2% increase since the industrialisation in 2011 (Lei et al.,

Cite This Article:

Fahriansyah, I., Khatrin, I., Abdullah, I., & Krisnandi, Y. K. (2024). Amine-modified Ni-DOBDC MOF for CO₂ capture: CO₂ adsorption capacity and reusability. *Environmental and Materials*, 2(2), 77-89. <https://doi.org/10.61511/eam.v2i2.2024.1431>

Copyright: © 2024 by the authors. This article is distributed under the terms and conditions of the Creative Commons Attribution (CC BY) license (<https://creativecommons.org/licenses/by/4.0/>).



2022a). The high levels of CO₂ emissions have been reported to increase the earth's temperature by approximately 1.05 °C, as reported by the Intergovernmental Panel on Climate Change (IPCC), which causing the rise of sea levels of 62.3 mm, according to the International Monetary Fund (IMF) in 2022 (Qasem et al., 2018). Furthermore, rising CO₂ could also affect marine ecosystems, particularly for shell-forming organisms. Since CO₂ increased ocean acidity due to the dissolution of CO₂ in seawater, causing a shortage of carbonate ions as the calcium carbonate (CaCO₃) salts tend to be converted into bicarbonate ions (HCO₃⁻) (Choe et al., 2021).

The extensive use of fossil fuels has caused significant negative impacts toward environment, initiating researchers to develop technologies to capture CO₂. There has been reported several methods, including cryogenic distillation, chemical adsorption and physical adsorption (Adhikari & Lin, 2016; Chen et al., 2021). Adsorption has remain a promising candidate among various technologies due to its high energy efficiency and low operational costs (Huang et al., 2014). Physical adsorption using porous solid materials as adsorbents is widely used for CO₂ capture, including a variety of of adsorbents such as zeolite, polymers, carbons and Metal Organic Frameworks (MOFs) (Sin et al., 2019). Despite the cost-effectiveness and optimised result offered by zeolites and carbons, the exceptional porosity and chemical tunability of MOFs have gain massive attention to replace both materials (Herm et al., 2012). Due to the large surface areas, low density, tunable porosity, and selective affinity towards specific gases, MOFs exhibit promising applications as storage media and separation adsorbents (Adhikari & Lin, 2016; Basu et al., 2011). Furukawa *et al.* reported the highest specific area MOF-210 to date (6240 m²g⁻¹), which exhibits exceptional CO₂ capture ability up to 71% at 50 bar and 298 K (Furukawa et al., 2010). Additionally, MOF-177 also showed high CO₂ adsorption capacity of 60% at 35 bar, according to Adhikari & Lin (Adhikari & Lin, 2016).

MOFs based on 2,5-dihydroxyterephthalate acid (DOBDC) linkers have demonstrated high CO₂ adsorption, favourable structural characteristics, and large surface areas. Numerous modifications towards DOBDC MOF have been reported in order to improve the CO₂ adsorption capacity, these include of the metal sites and the addition of functional groups. In terms of metal sites, Ni-based DOBDC MOF has been reported to be more effective for CO₂ adsorption (Adhikari & Lin, 2016; Ghanbari et al., 2020; Kalyon et al., 2024; Liu et al., 2023). Liu *et al.* on their findings indicated that Ni/DOBDC MOF is more stable compared to Mg/DOBDC MOF due to the higher oxidation susceptibility of Mg (Liu et al., 2023), while Adhikari *et al.* reported that Ni-based MOFs exhibit higher CO₂ adsorption capacity (11.06 mmol) compared to Co-based MOFs (10.28 mmol) (Adhikari & Lin, 2016). In terms of the addition of functional groups, polar functional groups like -OH, -N=N-, -NH₂, and -N=C(R)- have been reported to enhanced CO₂ adsorption capacity due to the quadrupole moment of CO₂ molecules (Ghanbari et al., 2020; Kalyon et al., 2024).

In this study, Ni-based DOBDC MOF synthesised *via* solvothermal method is being modified with a variation of ethylenediamine (EDA) concentration to improve the CO₂ adsorption capacity. A series of characterisation using XRD, FT-IR, N₂-physisorption, and SEM-EDX were carried out to study the physicochemical properties of the as-synthesised Ni-DOBDC and EDA/Ni-DOBDC. Furthermore, CO₂ adsorption tests were carried out and quantitatively analysed using titration method. Temperature and CO₂ concentration were modified to obtain the optimum adsorption condition, which further used to the analysis of reusability of both adsorbents. To the best of author knowledge, analysis of the EDA concentrations towards the CO₂ adsorption capacity and reusability is yet to be reported.

2. Methods

2.1 Materials

The materials used in this research, including distilled water, were used without further purification, including 2,5-dihydroxyrephthalic acid (DOBDC, 98%), nickel (II) nitrate hexahydrate (Ni(NO₃)₂·6H₂O, for analysis EMSURE® ACS), *N,N*-dimethylformamide

(DMF, anhydrous, 99.8%), 1,2-diaminoethane (ethylenediamine, ReagentPlus®, ≥99%), sodium hydroxide (NaOH, 0.1 N solution), hydrochloric acid (HCl, 37%, ACS reagent), potassium hydrogen phthalate (KHP, for analysis EMSURE® Reag. Ph Eur), methanol (absolute), ethanol (absolute), phenolphthalein (indicator, ACS reagent), and methyl orange (indicator pH 3.0-4.4), which were obtained from Sigma Aldrich. CO₂ (Ultra High Purity, 99.99%) and N₂ (Ultra High Purity, 99.99%) gasses were obtained from CV Retno Gas (Jakarta, Indonesia).

2.2 Adsorbent synthesis and modification

Ni-based MOF was synthesised following procedure from Li *et al.*, with some modifications (Li *et al.*, 2014). The synthesis involved the addition of 0.48 g DOBDC and 2.38 g nickel(II) nitrate hexahydrate to a mixture of 50 mL DMF, 50 mL ethanol, and 50 mL distilled water. The mixture was then stirred and sonicated for 30 mL at room temperature. The resulting solution was then transferred to a teflon-lined autoclave and heated at 100 °C for 24 h in an oven. The obtained yellowish-brown precipitate was filtered, washed with methanol, and dried to achieve Ni-DOBDC.

Modification of Ni-DOBDC MOF with ethylenediamine (EDA) was carried out following procedure from Easun *et al.*, with some modifications (Asghar *et al.*, 2020a). Initially, 0.1 g Ni-DOBDC MOF was prepared and added to EDA in ethanol solutions with variations of concentration of 10%, 15%, and 20%. The mixture was then subjected to reflux heating with stirring at 400-450 rpm for 8 h at 70 °C. The resulting product was filtered and washed sequentially with deionised water and ethanol. The sample was dried at room temperature for 24 hours to produce a EDA/Ni-DOBDC x , with x as the concentration of EDA.

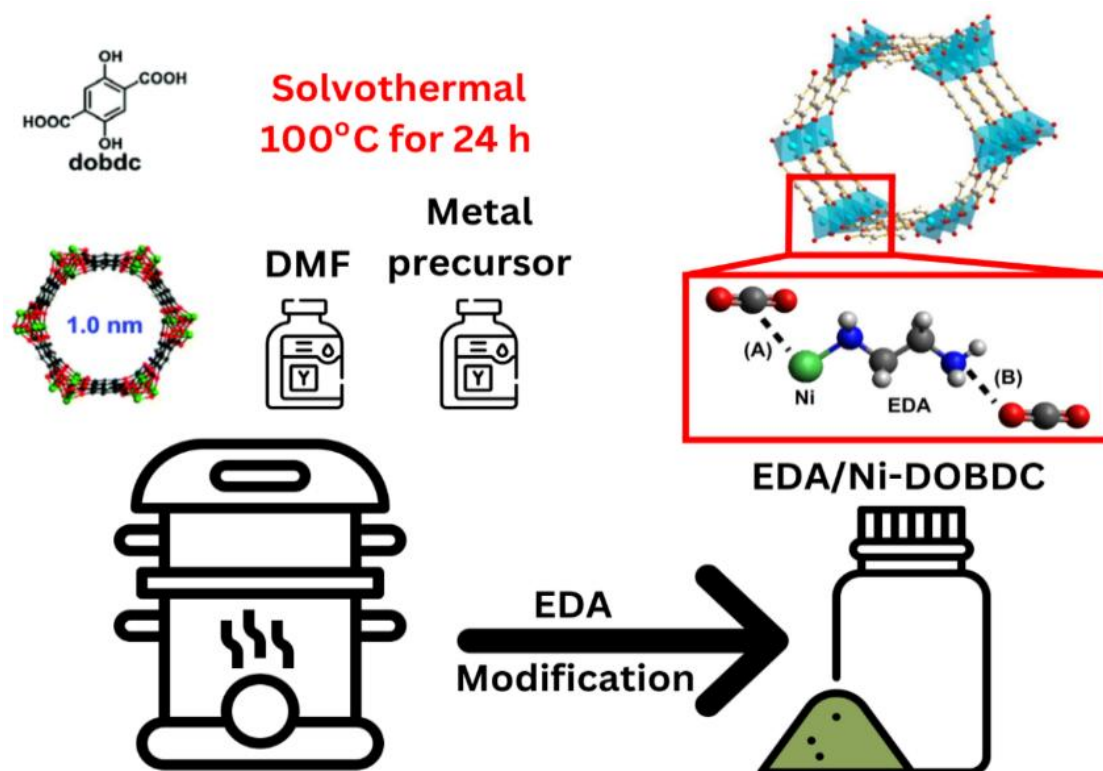


Fig. 1. Schematic illustration of EDA/Ni-DOBDC synthesis

2.3 Characterisation method

The structure and crystallinity of Ni-DOBDC MOF and its modifications were determined using an X-ray diffraction diffractometer (PANalytical Empyrean) operated at 40 kV and 30 mA, with a K α radiation source ($\lambda = 1.54059 \text{ \AA}$) over 2θ range of 5–90°.

Functional group identification was conducted using an Alpha-Bruker Fourier Transform Infrared (FT-IR) spectrometer with a resolution of 4 cm^{-1} , utilising potassium bromide (KBr) pellets. Textural properties of adsorbents were investigated using surface area and pore analyser (Quantachrome Quadrasorb-Evo) with N_2 gas using Brunauer-Emmett-Teller (BET) method and BJH method for pore size analysis. Morphology analysis was conducted via SEM imaging using JEOL-JSM-6510LA Scanning Electron Microscope equipped with Energy Dispersive X-ray (EDX).

2.4 Adsorption test

The CO_2 adsorption test was conducted following the procedure from our previous studies (Lestari et al., 2018). Prior to the adsorption test, the adsorbent was heated in a tubular furnace at $60\text{ }^\circ\text{C}$ for 1 h under N_2 conditions. Adsorption tests were performed in a chamber connected to a closed container containing 100 mL NaOH solution ($1 \times 10^{-5}\text{ M}$, $\pm 2\text{ }^\circ\text{C}$). 0.05 g of adsorbent was placed in the chamber and flowed with CO_2 gas with a duration ranging from 5 to 30 mins. Optimum adsorption condition was investigated by modifying the adsorption temperature (25, 50, and $75\text{ }^\circ\text{C}$) and CO_2 concentration (40 and 50% in N_2).

The CO_2 concentration in NaOH solution was determined via titration method as described in (Kim et al., 2005). A 10 mL sample of NaOH- CO_2 solution was titrated with $1 \times 10^{-5}\text{ M}$ HCl solution. Titration to the first equivalence point was noted by a colour change of PP indicator to colourless, indicative of the neutralisation of the excess NaOH and conversion of sodium carbonate to sodium bicarbonate. Titration to second equivalent point utilised methyl orange indicator, which indicated the conversion of sodium bicarbonate into CO_2 and H_2O . The concentration of dissolved CO_2 was calculated based on the difference in titrant volume between the first and second equivalence points. The reusability test was carried out in three cycles following the procedure from Li et al., with some modifications (Li et al., 2014). Following the CO_2 adsorption test, the sample was degassed with N_2 at $100\text{ }^\circ\text{C}$ for 30 mins.

The amount of CO_2 adsorbed onto MOF materials was determined by comparing the molar difference of CO_2 in a blank experiment (without adsorbent) and in the NaOH solution for each experiment. HCl solution used was standardised with a $1 \times 10^{-5}\text{ M}$ KHP solution to ensure accuracy in the calculation. Similarly, $1 \times 10^{-5}\text{ M}$ NaOH solution was standardised with HCl standard solution. The calculation of CO_2 adsorption was performed using Eq. 1-3.

$$\text{Mol of CO}_2 \text{ passing through the adsorbent} = \text{Mol of CO}_2 \text{ in NaOH solution} \quad (\text{Eq. 1})$$

$$\text{Mol of CO}_2 \text{ in NaOH solution} = \frac{1}{2} \{ \text{mol of NaOH} - (\text{M HCl} \times \Delta V \text{ HCl}) \} \quad (\text{Eq. 2})$$

$$\text{Mol of CO}_2 \text{ adsorbed} = \text{mol of CO}_2 \text{ (blank)} - \text{mol of CO}_2 \text{ passing through adsorbent} \quad (\text{Eq. 3})$$

3. Results and Discussion

3.1 Adsorbent characterisations

XRD patterns of Ni-DOBDC and its EDA derivatives are presented in Fig. 2a-b. Fig. 2 compares the XRD pattern of the as-synthesised Ni-DOBDC and Ni-DOBDC reference (CCDC No. 288477) (Zhou et al., 2024). Two prominent peaks were observed at $2\theta = 6.8^\circ$ and 11.8° associated with the (110) and (300) plane, respectively. The as-synthesised Ni-DOBDC pattern also shows similarities with the diffraction patterns of previously reported studies from Li et al. and Song et al. (Li et al., 2014; Song et al., 2022). Based on the similarities of XRD patterns with reference and previous studies, it can be concluded that the crystalline structure of the as-synthesised Ni-DOBDC was successfully formed.

Fig. 2b depicts the XRD patterns of the as-synthesised Ni-DOBDC and its EDA-derivatives. EDA/Ni-DOBDC 10% shows similar patterns to the pristine Ni-DOBDC with a slight shift along the x-axis, which is likely caused by the addition of EDA groups. These

results indicated that the addition of 10% EDA did not damage or degrade the crystalline structure of Ni-DOBDC. In contrast, the diffraction patterns of EDA/Ni-DOBDC 15% and 20% displayed no detectable peaks. This absence is likely due to the disruption or collapse of the framework structure of Ni-DOBDC due to the excessive concentration of EDA (Daud et al., 2022). Furthermore, Table 1 presents the analysis of XRD result using Scherrer equation to investigate the crystallite size. Ni-DOBDC exhibits crystallite with average size of 0.12 μm , while modification with EDA decreased the crystallite size of EDA/Ni-DOBDC to 0.09 μm .

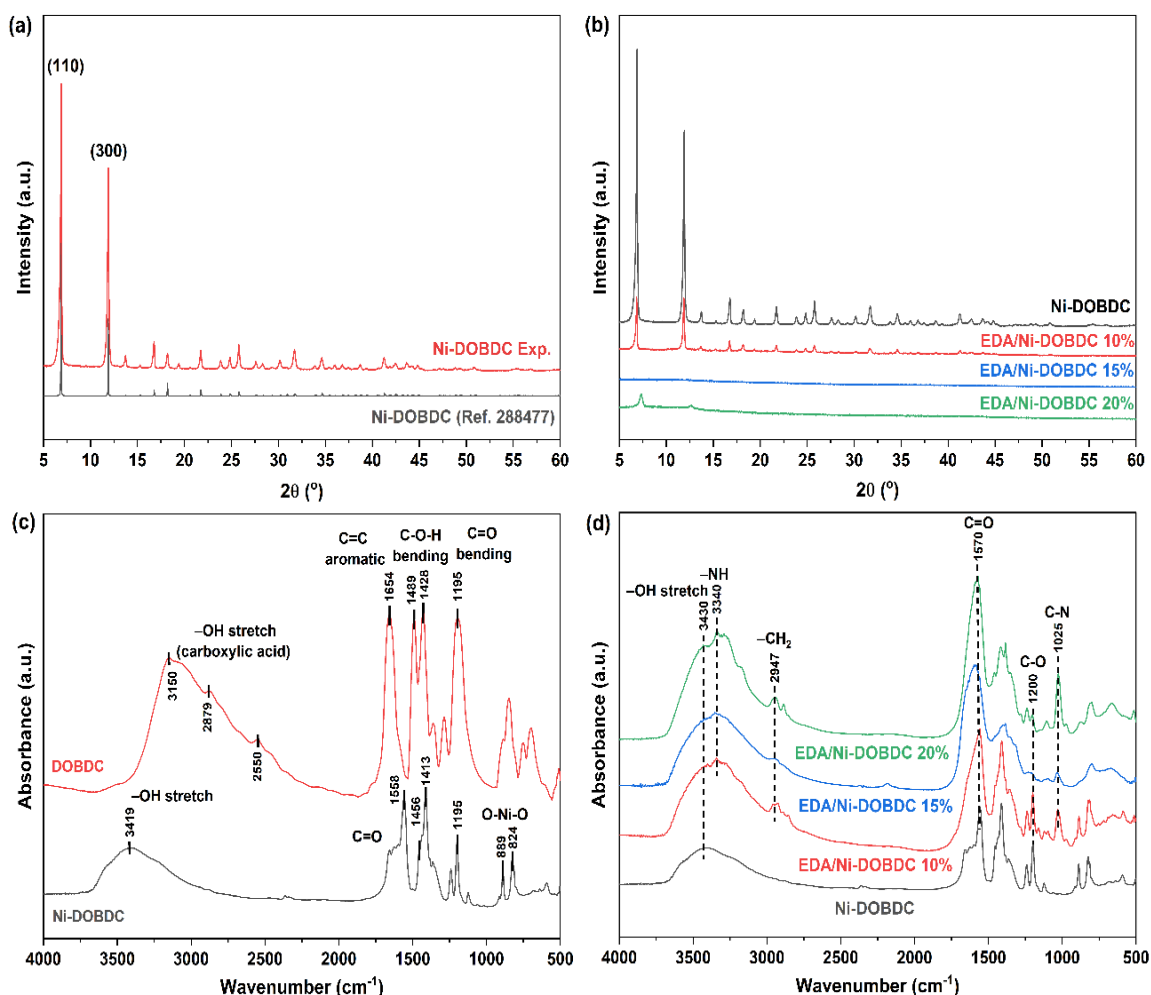


Fig. 2. XRD patterns of (a) Ni-DOBDC and (b) Ni-DOBDC and its EDA derivatives; FT-IR spectra of (c) Ni-DOBDC and (d) Ni-DOBDC and its EDA derivatives

The FTIR spectrum of the as-synthesized Ni-DOBDC (Fig. 2c) revealed several characteristic peaks, including -OH vibration at 3419 cm^{-1} , C=O stretching peak at 1658 cm^{-1} , aromatic C=C group at 1413 cm^{-1} , and C=O group at 1195 cm^{-1} (Pamei et al., 2022), originating from the DOBDC ligand bound to the metal (Asghar et al., 2020b; Lei et al., 2022b). The FT-IR spectrum of the as-synthesised Ni-DOBDC was compared with both the reference spectrum for Ni-DOBDC and DOBDC ligand, which demonstrated consistency between the as-synthesised Ni-DOBDC and the reference Ni-DOBDC MOF, as well as the ligand. No significant changes were investigated, only differences are in -OH vibration and additional peak of O-Ni-O at 889 and 824 cm^{-1} . Additionally, new peaks corresponding to -NH , -NH_2 , and C-N groups were observed in EDA/Ni-DOBDC samples (Fig. 2d) due to the incorporation of EDA groups into MOF framework. FT-IR analysis of Ni-DOBDC supports the successful formation of the Ni-DOBDC MOF as shown by XRD patterns.

EDA/Ni-DOBDC 10% will be used for further characterisation and adsorption test since XRD and FT-IR results show that the addition of 15% and 20% EDA caused the breakdown

of Ni-DOBDC framework. Table 1 presents the N_2 -physisorption results of Ni-DOBDC and its EDA-derivative, with the decrease of S_{BET} of EDA/Ni-DOBDC as compared to Ni-DOBDC ($257 \text{ m}^2 \text{ g}^{-1}$). However, V_{total} and pore diameter of EDA/Ni-DOBDC was retained as shown by its similarities with pristine Ni-DOBDC. The decrease of EDA/Ni-DOBDC surface area might be due to the incorporation of EDA into the pores of Ni-DOBDC, since XRD results show no breakdown of the structure of EDA/Ni-DOBDC 10%.

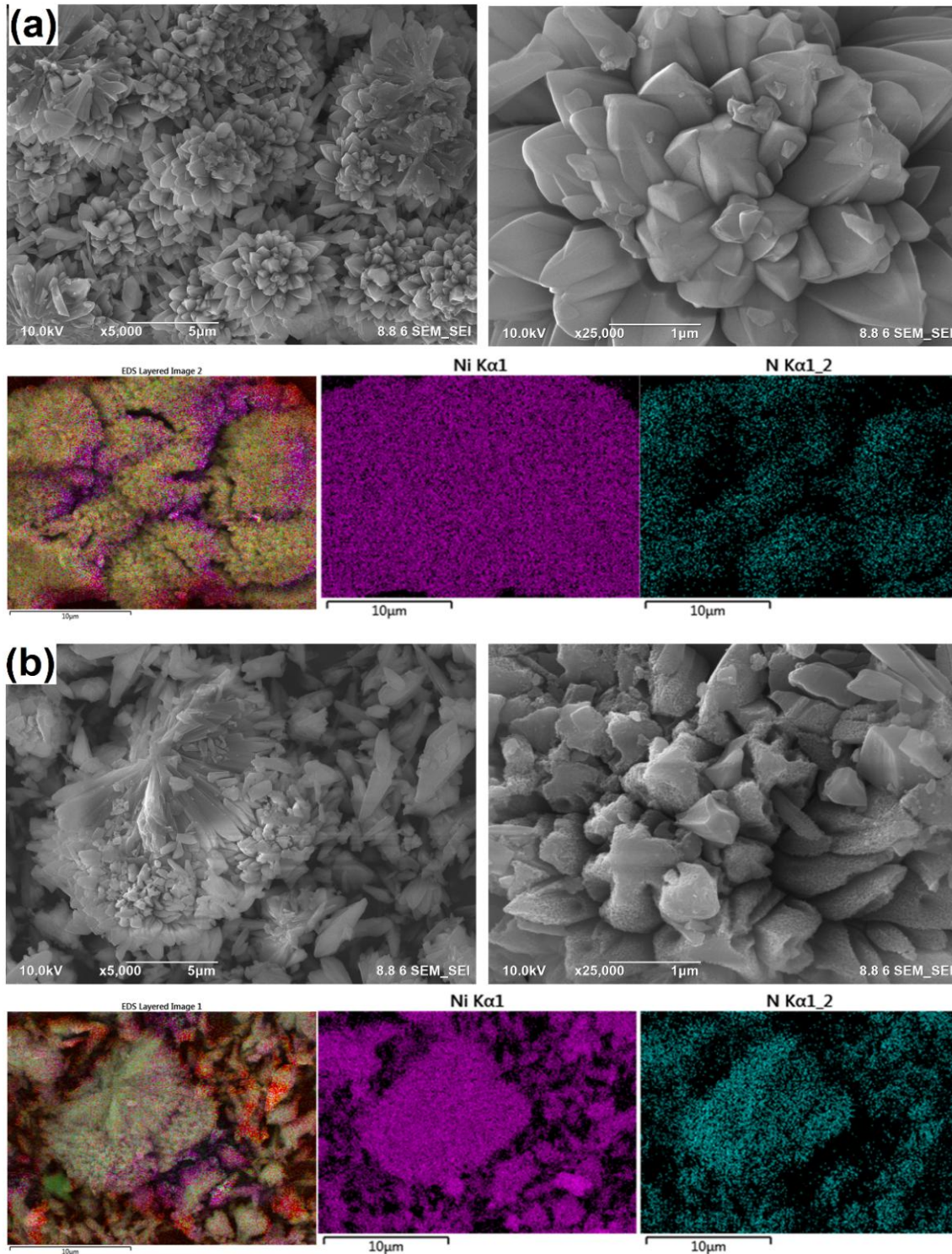


Fig. 3. SEM images of (a) Ni-DOBDC and (b) EDA/Ni-DOBDC 10% with their representative EDX mapping of full elements, Ni, and N only

Fig. 3 presents the SEM-EDX images of Ni-DOBDC (Fig. 3a) and EDA/Ni-DOBDC (Fig. 3b), with their representative mapping of full elements, Ni, and N. SEM images of Ni-DOBDC show a rod morphology aggregated into a flower-like structure with an average particle size of 0.75 μm . These results show similarities with our previous studies and study from Chen *et al.* (Chen *et al.*, 2019, 2022). The addition of EDA did not change the overall morphology of EDA/Ni-DOBDC, only an increased in an average particle size of 0.87 μm was observed. Furthermore, mapping results show a great distribution of Ni and N elements within both materials, while EDA analysis (Table 1) shows a decrease in Ni wt.% after modification of Ni-DOBDC with EDA. These results might be indicative of the successful incorporation of EDA into Ni-DOBDC framework, despite the unavailability of EDX method to provide the wt.% of N element (Wolfgong, 2016).

Table 1. Textural properties and composition of Ni-DOBDC and EDA/Ni-DOBDC

Sample	Particle size		Wt. % ^b		S_{BET} ($\text{m}^2 \text{g}^{-1}$) ^c	V_{total} ($\text{cm}^3 \text{g}^{-1}$) ^d	Pore d (nm) ^e
	Crystallite ^a	Crystal ^b	Ni	N			
Ni-DOBDC	0.12 μm	0.75 μm	26	0	257	0.248	3.4; 4.8; 7.2
EDA/Ni-DOBDC	0.09 μm	0.87 μm	19	0	0	0.248	3.4

^a Determined using Scherrer equation by XRD pattern of $2\theta = 6.8^\circ$ and 11.8° .

^b Determined using SEM-EDX.

^c Determined using BET method.

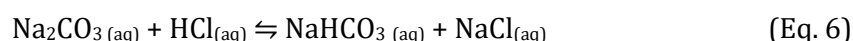
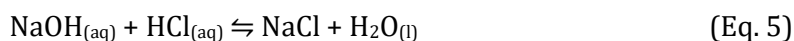
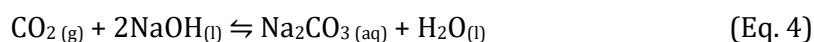
^d Determined at $p/p_0 = 0.99$.

^e Determined using BJH method.

3.2 Adsorption test

The effect of EDA incorporation into Ni-DOBDC MOF as CO_2 capture was studied in terms of the CO_2 adsorption and reusability. The optimum condition for the adsorption test was investigated by altering the adsorption temperature and concentration of CO_2 . Adsorption test was carried out in a chamber connected to a closed container containing NaOH solution.

The CO_2 concentration in NaOH solution was then determined *via* titration method following our previous studies (Faisal *et al.*, 2021; Lestari *et al.*, 2018). Eq. 4 described the reaction between CO_2 and NaOH at the end of the reaction chamber. A 10 mL sample of NaOH- CO_2 solution was titrated with 1×10^{-5} M HCl solution following the reaction in Eq. 5 and Eq. 6. Titration to the first equivalence point was noted by a colour change of PP indicator to colourless, indicating the neutralisation of the excess NaOH and conversion of sodium carbonate to sodium bicarbonate. Titration to the second equivalent point utilised methyl orange indicator, which indicated the conversion of sodium bicarbonate into CO_2 and H_2O (Eq. 7). The concentration of dissolved CO_2 was calculated based on the difference in titrant volume between the first and second equivalence points.



3.2.1 Effect of temperature

Fig. 4a presents the CO_2 adsorption capacity of Ni-DOBDC at varying temperatures: 25 $^\circ\text{C}$, 50 $^\circ\text{C}$, and 70 $^\circ\text{C}$. The results indicate that the adsorption capacity of Ni-DOBDC MOF increases with rising temperature. This trend could be attributed to the additional external energy provided at higher temperatures, which strengthens the interaction between CO_2 molecules and the active sites within the Ni-DOBDC MOF. Another potential explanation is

that higher temperatures enhance the vibrational motion of CO₂, increasing its polarity and, consequently, its interaction with the MOF. Furthermore, the graph also reveals that, across all temperatures, the adsorption capacity rises steadily from minute 5 to minute 20, followed by a decline at the minute 30. This decrease may occur due to saturation of the MOF's adsorption sites, which limits further CO₂ uptake after 30 minutes. Similar to Ni-DOBDC, the adsorption capacity of EDA/Ni-DOBDC (Fig. 4b) increases with temperature, in which the CO₂ adsorption capacity increases from minute 5 to minute 20, followed by a decline at minute 30 due to the saturation of the MOF adsorption sites.

A comparison of the adsorption graphs for Ni-DOBDC and EDA/Ni-DOBDC shows that EDA/Ni-DOBDC consistently exhibits a higher adsorption capacity at all temperature conditions. This improvement might be attributed to the presence of EDA, which interacts with CO₂ to form carbamate compounds. In contrast, the adsorption mechanism of Ni-DOBDC MOF is limited to interactions between CO₂ with the metal and ligand sites of pristine Ni-DOBDC.

3.2.2 Effect of CO₂ concentration

The effect of CO₂ concentration was conducted using 40% and 50% CO₂ in N₂ mixture at the optimum adsorption temperature of 70 °C. At 40% CO₂ concentration (Fig. 4c), the adsorption capacity of Ni-DOBDC shows a small increase from minute 5 to 20, followed by a sharp rise between minutes 20 and 30. These results indicated that during the earlier stage (5 – 20 min), the adsorbent only adsorbed a small amount of CO₂ with a significant increase in CO₂ uptake at 30 min adsorption time. While at 50% CO₂ concentrations, the adsorption capacity of Ni-DOBDC increases until minute 20 and decreases after the saturation of the MOF adsorption sites. On the other hand, at 40% and 50% CO₂ concentration, the adsorption capacity of EDA/Ni-DOBDC (Fig. 4d) steadily increases until minute 30, which might be indicative of the saturation point of the EDA/Ni-DOBDC adsorption sites that are not reached yet.

3.2.3 Reusability test

The reusability test was conducted to assess the adsorption capacity percentage of Ni-DOBDC and EDA/Ni-DOBDC after multiple uses. Reusability tests of both Ni-DOBDC and EDA/Ni-DOBDC MOF were carried out at the obtained optimum condition of temperature 70 °C and CO₂ concentration of 50%. Prior to the test, the samples were treated physically with N₂ gas to remove any residual CO₂ remaining on the surface and within the pores. The samples were then heated to 100°C to eliminate water vapour and any other compounds.

Fig. 4e shows the reusability test of Ni-DOBDC MOF over three cycles. By considering the adsorption capacity of the first cycle as 100% (6.44 mmol g⁻¹), a decrease in the adsorption capacity of 67% and 47% was observed after the second and third cycles, respectively. On the other hand, the reusability test of EDA/Ni-DOBDC (Fig. 4f) shows high CO₂ adsorption capacity to Ni-DOBDC (9.95 mmol g⁻¹) with a decrease to 49% and 28% after second and third cycle, respectively. These results indicated that pristine Ni-DOBDC possesses better reusability up to three cycles compared to its EDA derivative, which might undergo EDA leaching throughout the adsorption process. However, it is also worth noting that the physical treatment of used adsorbent with N₂ gas might not be fully effective in desorbing CO₂ from MOF structure.

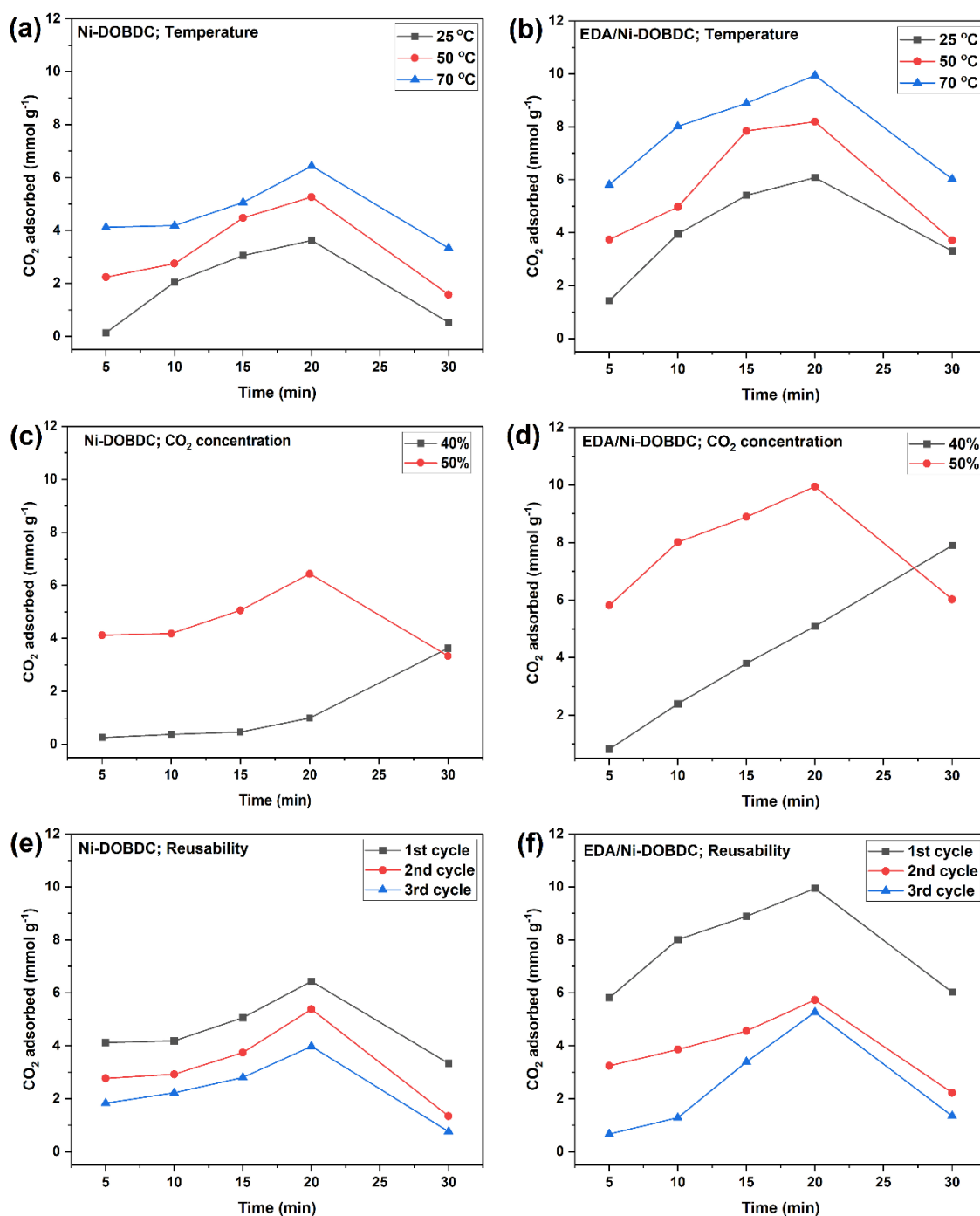


Fig. 4. CO₂ adsorption capacity of (a) Ni-DOBDC and (b) EDA/Ni-DOBDC at atmospheric pressure with a variation of temperature; CO₂ adsorption capacity of (c) Ni-DOBDC and (d) EDA/Ni-DOBDC at atmospheric pressure with a variation of CO₂ concentration; also Reusability of (e) Ni-DOBDC and (f) EDA/Ni-DOBDC with 50% CO₂ at 70 °C and atmospheric pressure

4. Conclusions

Ni-DOBDC MOF has been successfully synthesised as confirmed by the characteristic peaks of XRD at $2\theta = 6.8^\circ$ and 11.8° and FT-IR results. The incorporation of 10% EDA into the MOF framework was also confirmed by no structural changes from XRD patterns. However, an increase in EDA concentration to 15% and 20% is causing a breakdown in the Ni-DOBDC framework. The incorporation of EDA into Ni-DOBDC pores was denoted by the decrease in surface area after EDA modification. SEM-EDX analysis confirms the flower-like rod aggregate morphology of the Ni-DOBDC and EDA/Ni-DOBDC MOFs, as well as the

increase of average particle size from 0.75 μm to 0.87 μm after EDA modification. The CO_2 adsorption tests conclude that the addition of EDA enhances the CO_2 adsorption capacity of Ni-DOBDC. However, the reusability test shows that pristine Ni-DOBDC possesses a better reusability than EDA/Ni-DOBDC after three cycles with physical treatment using N_2 between each cycle.

Acknowledgement

The authors express their gratitude to the reviewers for their valuable and constructive feedback on this article.

Author Contribution

Conceptualization, I.A. and Y.K.K.; Methodology, I.A. and Y.K.K.; Validation, I.F. and I.K.; Formal Analysis, I.F.; Investigation, I.F.; Data Curation, I.F. and I.K.; Writing – Original Draft Preparation, I.K.; Writing – Review & Editing, I.K. and Y.K.K.; Visualization, I.F. and I.K.; Supervision, I.A. and Y.K.K.; Project Administration, I.K.; and Funding Acquisition, Y.K.K.

Funding

Universitas Indonesia funded this research through Hibah Publikasi Terindeks Internasional (PUTI) Q2 Research Grant No. NKB-781/UN2.RST/HKP.05.00/2023.

Ethical Review Board Statement

Not available.

Informed Consent Statement

Not available.

Data Availability Statement

Not available.

Conflicts of Interest

The authors declare no conflict of interest.

Open Access

©2024. The author(s). This article is licensed under a Creative Commons Attribution 4.0 International License, which permits use, sharing, adaptation, distribution and reproduction in any medium or format, as long as you give appropriate credit to the original author(s) and the source, provide a link to the Creative Commons license, and indicate if changes were made. The images or other third-party material in this article are included in the article's Creative Commons license, unless indicated otherwise in a credit line to the material. If material is not included in the article's Creative Commons license and your intended use is not permitted by statutory regulation or exceeds the permitted use, you will need to obtain permission directly from the copyright holder. To view a copy of this license, visit: <http://creativecommons.org/licenses/by/4.0/>

References

- Adhikari, A. K., & Lin, K. S. (2016). Improving CO_2 adsorption capacities and CO_2/N_2 separation efficiencies of MOF-74(Ni, Co) by doping palladium-containing activated carbon. *Chemical Engineering Journal*, 284, 1348–1360. <https://doi.org/10.1016/j.cej.2015.09.086>
- Asghar, A., Iqbal, N., Aftab, L., Noor, T., Kariuki, B. M., Kidwell, L., & Easun, T. L. (2020a). Ethylenediamine loading into a manganese-based metal–organic framework enhances water stability and carbon dioxide uptake of the framework. *Royal Society Open Science*, 7(3). <https://doi.org/10.1098/RSOS.191934>

- Asghar, A., Iqbal, N., Noor, T., & Khan, J. (2020b). Ethylenediamine (EDA) loading on MOF-5 for enhanced carbon dioxide capture applications. *IOP Conference Series: Earth and Environmental Science*, 471(1), 012009. <https://doi.org/10.1088/1755-1315/471/1/012009>
- Basu, S., Cano-Odena, A., & Vankelecom, I. F. J. (2011). MOF-containing mixed-matrix membranes for CO₂/CH₄ and CO₂/N₂ binary gas mixture separations. *Separation and Purification Technology*, 81(1), 31–40. <https://doi.org/10.1016/J.SEPPUR.2011.06.037>
- Chen, C., Feng, X., Zhu, Q., Dong, R., Yang, R., Cheng, Y., & He, C. (2019). Microwave-Assisted Rapid Synthesis of Well-Shaped MOF-74 (Ni) for CO₂ Efficient Capture. *Inorganic Chemistry*, 58(4), 2717–2728. <https://pubs.acs.org/doi/abs/10.1021/acs.inorgchem.8b03271>
- Chen, C., Kosari, M., Jing, M., & He, C. (2022). Microwave-assisted synthesis of bimetallic NiCo-MOF-74 with enhanced open metal site for efficient CO₂ capture. *Environmental Functional Materials*, 1(3), 253–266. <https://doi.org/10.1016/J.EFMAT.2023.01.002>
- Chen, S., Li, X., Duan, J., Fu, Y., Wang, Z., Zhu, M., & Li, N. (2021). Investigation of highly efficient adsorbent based on Ni-MOF-74 in the separation of CO₂ from natural gas. *Chemical Engineering Journal*, 419, 129653. <https://doi.org/10.1016/J.CEJ.2021.129653>
- Choe, J. H., Kim, H., & Hong, C. S. (2021). MOF-74 type variants for CO₂ capture. *Materials Chemistry Frontiers*, 5(14), 5172–5185. <https://doi.org/10.1039/D1QM00205H>
- Daud, A. D., Lim, H. N., Ibrahim, I., Endot, N. A., Gowthaman, N. S. K., Jiang, Z. T., & Cordova, K. E. (2022). An effective metal-organic framework-based electrochemical non-enzymatic glucose sensor. *Journal of Electroanalytical Chemistry*, 921, 116676. <https://doi.org/10.1016/J.JELECHEM.2022.116676>
- Faisal, M., Pamungkas, A. Z., & Krisnandi, Y. K. (2021). Study of Amine Functionalized Mesoporous Carbon as CO₂ Storage Materials. *Processes*, 9(3), 456. <https://doi.org/10.3390/pr9030456>
- Furukawa, H., Ko, N., Go, Y. B., Aratani, N., Choi, S. B., Choi, E., Yazaydin, A. Ö., Snurr, R. Q., O’Keeffe, M., Kim, J., & Yaghi, O. M. (2010). Ultrahigh porosity in metal-organic frameworks. *Science*, 329(5990), 424–428. <https://www.science.org/doi/abs/10.1126/science.1192160>
- Ghanbari, T., Abnisa, F., & Wan Daud, W. M. A. (2020). A review on production of metal organic frameworks (MOF) for CO₂ adsorption. *Science of The Total Environment*, 707, 135090. <https://doi.org/10.1016/J.SCITOTENV.2019.135090>
- Herm, Z. R., Krishna, R., & Long, J. R. (2012). CO₂/CH₄, CH₄/H₂ and CO₂/CH₄/H₂ separations at high pressures using Mg₂(dobdc). *Microporous and Mesoporous Materials*, 151, 481–487. <https://doi.org/10.1016/J.MICROMESO.2011.09.004>
- Huang, W., Zhou, X., Xia, Q., Peng, J., Wang, H., & Li, Z. (2014). Preparation and Adsorption Performance of GrO@Cu-BTC for Separation of CO₂/CH₄. *Industrial and Engineering Chemistry Research*, 53(27), 11176–11184. <https://doi.org/10.1021/IE501040S>
- Kalyon, H. Y., Yilmaz, O., Gencten, M., Gorduk, S., & Sahin, Y. (2024). Ethylenediamine-functionalized metal-organic frameworks for applications of electrochemical supercapacitors as an additive. *Synthetic Metals*, 306, 117627. <https://doi.org/10.1016/J.SYNTHMET.2024.117627>
- Kim, D. J., Lee, H. I., Yie, J. E., Kim, S. J., & Kim, J. M. (2005). Ordered mesoporous carbons: Implication of surface chemistry, pore structure and adsorption of methyl mercaptan. *Carbon*, 43(9), 1868–1873. <https://doi.org/10.1016/J.CARBON.2005.02.035>
- Lei, L., Cheng, Y., Chen, C., Kosari, M., Jiang, Z., & He, C. (2022a). Taming structure and modulating carbon dioxide (CO₂) adsorption isosteric heat of nickel-based metal organic framework (MOF-74(Ni)) for remarkable CO₂ capture. *Journal of Colloid and Interface Science*, 612, 132–145. <https://doi.org/10.1016/J.ICIS.2021.12.163>
- Lei, L., Cheng, Y., Chen, C., Kosari, M., Jiang, Z., & He, C. (2022b). Taming structure and modulating carbon dioxide (CO₂) adsorption isosteric heat of nickel-based metal organic framework (MOF-74(Ni)) for remarkable CO₂ capture. *Journal of Colloid and Interface Science*, 612, 132–145. <https://doi.org/10.1016/J.ICIS.2021.12.163>

- Lestari, W. W., Wibowo, A. H., Astuti, S., Irwinsyah, Pamungkas, A. Z., & Krisnandi, Y. K. (2018). Fabrication of hybrid coating material of polypropylene itaconate containing MOF-5 for CO₂ capture. *Progress in Organic Coatings*, 115, 49–55. <https://doi.org/10.1016/J.PORGCOAT.2017.11.006>
- Li, L., Yang, J., Li, J., Li, J., & Chen, Y. (2014). Separation of CO₂/CH₄ and CH₄/N₂ mixtures by M/DOBDC: A detailed dynamic comparison with MIL-100(Cr) and activated carbon. *Microporous and Mesoporous Materials*, 198, 236–246. <https://doi.org/10.1016/J.MICROMESO.2014.07.041>
- Liu, F., Wang, T., Dong, H., & Liu, W. (2023). Modified metal–organic framework by a novel coordinatively unsaturated amine grafting mechanism for direct air capture of CO₂. *Chemical Engineering Journal*, 454, 140431. <https://doi.org/10.1016/J.CEJ.2022.140431>
- Pamei, M., Kumar, S., Achumi, A. G., & Puzari, A. (2022). Supercapacitive amino-functionalized cobalt and copper metal-organic frameworks with varying surface morphologies for energy storage. *Journal of Electroanalytical Chemistry*, 924, 116885. <https://doi.org/10.1016/J.JELECHEM.2022.116885>
- Qasem, N. A. A., Ben-Mansour, R., & Habib, M. A. (2018). An efficient CO₂ adsorptive storage using MOF-5 and MOF-177. *Applied Energy*, 210, 317–326. <https://doi.org/10.1016/J.APENERGY.2017.11.011>
- Sin, M., Kavooosi, N., Rauche, M., Pallmann, J., Paasch, S., Senkovska, I., Kaskel, S., & Brunner, E. (2019). In Situ 13 C NMR Spectroscopy Study of CO₂/CH₄ Mixture Adsorption by Metal-Organic Frameworks: Does Flexibility Influence Selectivity? *Langmuir*, 35(8), 3162–3170. <https://pubs.acs.org/doi/abs/10.1021/acs.langmuir.8b03554>
- Song, K., Liang, S., Zhong, X., Wang, M., Mo, X., Lei, X., & Lin, Z. (2022). Tailoring the crystal forms of the Ni-MOF catalysts for enhanced photocatalytic CO₂-to-CO performance. *Applied Catalysis B: Environmental*, 309, 121232. <https://doi.org/10.1016/J.APCATB.2022.121232>
- Stolar, T., Prašnikar, A., Martinez, V., Karadeniz, B., Bjelić, A., Mali, G., Friščić, T., Likozar, B., & Užarević, K. (2021). Scalable mechanochemical amorphization of bimetallic Cu-Zn MOF-74 catalyst for selective CO₂ reduction reaction to methanol. *ACS Applied Materials and Interfaces*, 13(2), 3070–3077. <https://pubs.acs.org/doi/abs/10.1021/acsami.0c21265>
- Ullah, S., Bustam, M. A., Al-Sehemi, A. G., Assiri, M. A., Abdul Kareem, F. A., Mukhtar, A., Ayoub, M., & Gonfa, G. (2020). Influence of post-synthetic graphene oxide (GO) functionalization on the selective CO₂/CH₄ adsorption behavior of MOF-200 at different temperatures; an experimental and adsorption isotherms study. *Microporous and Mesoporous Materials*, 296, 110002. <https://doi.org/10.1016/J.MICROMESO.2020.110002>
- Wolfgong, W. J. (2016). Chemical analysis techniques for failure analysis: Part 1, common instrumental methods. *Handbook of Materials Failure Analysis with Case Studies from the Aerospace and Automotive Industries*, 279–307. <https://doi.org/10.1016/B978-0-12-800950-5.00014-4>
- Zhou, J., Xu, L., Gai, H., Xu, N., Ren, Z., Hou, X., Chen, Z., Han, Z., Sarker, D., Levchenko, S. V., & Huang, M. (2024). Interpretable Data-Driven Descriptors for Establishing the Structure-Activity Relationship of Metal–Organic Frameworks Toward Oxygen Evolution Reaction. *Angewandte Chemie International Edition*, 63(36), e202409449. <https://doi.org/10.1002/ANIE.202409449>

Biographies of Authors

Irsan Fahriansyah, Department of Chemistry, Faculty of Mathematics and Natural Science, Universitas Indonesia, Depok, West Java 16424; and Solid Inorganic Framework Laboratory, Department of Chemistry, Faculty of Mathematic and Natural Sciences, Universitas Indonesia, Depok, West Java 16424, Indonesia.

- Email: irsanfahriansyah2620@gmail.com
- ORCID: N/A
- Web of Science ResearcherID: N/A
- Scopus Author ID: N/A
- Homepage: N/A

Irena Khatrin, Department of Chemistry, Faculty of Mathematics and Natural Science, Universitas Indonesia, Depok, West Java 16424; and Solid Inorganic Framework Laboratory, Department of Chemistry, Faculty of Mathematic and Natural Sciences, Universitas Indonesia, Depok, West Java 16424, Indonesia.

- Email: irena.khatrin@sci.ui.ac.id
- ORCID: 0000-0002-3490-0643
- Web of Science ResearcherID: N/A
- Scopus Author ID: 58077997600
- Homepage: <https://www.linkedin.com/in/irena-khatrin/>

Iman Abdullah, Department of Chemistry, Faculty of Mathematics and Natural Science, Universitas Indonesia, Depok, West Java 16424; and Solid Inorganic Framework Laboratory, Department of Chemistry, Faculty of Mathematic and Natural Sciences, Universitas Indonesia, Depok, West Java 16424; and Solid Inorganic Framework Laboratory, Department of Chemistry, Faculty of Mathematic and Natural Sciences, Universitas Indonesia, Depok, West Java 16424, Indonesia.

- Email: iman.abdullah@sci.ui.ac.id
- ORCID: 0000-0002-0612-0850
- Web of Science ResearcherID: N/A
- Scopus Author ID: 56973852800
- Homepage: <https://scholar.ui.ac.id/en/persons/iman-abdullah>

Yuni Krisyuningsih Krisnandi, Department of Chemistry, Faculty of Mathematics and Natural Science, Universitas Indonesia, Depok, West Java 16424; and Solid Inorganic Framework Laboratory, Department of Chemistry, Faculty of Mathematic and Natural Sciences, Universitas Indonesia, Depok, West Java 16424, Indonesia.

- Email: yuni.krisnandi@sci.ui.ac.id
- ORCID: 0000-0002-2753-5596
- Web of Science ResearcherID: N/A
- Scopus Author ID: 12761423100
- Homepage: <https://scholar.ui.ac.id/en/persons/yuni-krisyuningsih>